Supporting Information

Synthesis, structure and photoluminescence of Cu(I) complexes containing new functionalized 1,2,3-triazole ligands

Li-Xin Wang,[a] Shun-Cheung Cheng,[b] Yingying Liu,[c] Chi-Fai Leung,[d] Ji-Yan Liu,[a,*] Chi-Chiu Ko,[b,*] Tai-Chu Lau [b,*] and Jing Xiang,[a,*]

[a.] *Key Laboratory of Optoelectronic Chemical Materials and Devices (Ministry of Education), School of Optoelectronic Materials and Technology, Jianghan University, Wuhan, 430056 China. xiangjing35991@sohu.com*

[b.] *Department of Chemistry, City University of Hong Kong, Tat Chee Avenue, Kowloon Tong, Hong Kong.*

[c.] *Institute of Intelligent Machines, Hefei Institutes of Physical Science, Chinese Academy of Sciences, Hefei 230031, P. R. China.*

[d.] *Department of Science and Environmental Studies, The Education University of Hong Kong, Hong Kong, China.*

Table of Contents

Experimental Section

Physical Measurements and Instrumentation. ^{1}H NMR and $^{31}P\{^{1}H\}$ NMR spectra were recorded on a Bruker AV300 (300 MHz) FT-NMR spectrometer. Chemical shifts (δ, ppm) are reported relative to tetramethylsilane (Me_4Si). Elemental analysis was performed on an ElementarVario MICRO Cube elemental analyzer. IR spectra of the solid samples as KBr discs were obtained within the range 4000–400 cm^{-1} on an AVATAR 360 FTIR spectrometer. All of the electronic absorption spectra were recorded on a Hewlett–Packard 8453 or Hewlett– Packard 8452A diode-array spectrophotometer. Steady-state emission spectra were measured at room temperature and at 77 K on a Horiba JobinYvon Fluorolog-3-TCSPC spectrofluorometer. The solutions were rigorously degassed on a high-vacuum line in a two-compartment cell with not less than four successive freeze– pump–thaw cycles. The measurements at 77 K were carried out on dilute solutions of the samples in EtOH/MeOH (4:1, v/v) loaded in a quartz tube inside a quartz-walled Dewar flask that contained liquid nitrogen. Luminescence lifetimes were measured by using the time-correlated single-photon-counting (TCSPC) technique on a Fluorolog-3-TCSPC spectrofluorometer in a fast MCS mode with a Nano LED-375 LH excitation source, which had a peak excitation wavelength at 375 nm and a pulse width of less than 750 ps. Luminescent quantum yields for in the solution and the solid-state sample were determined using the integrating sphere assembly accessory (F-M01) of Edinburgh Instruments FLS980. The photon-counting data were analyzed on Horiba JobinYvon Decay Analysis Software.

X-ray Crystallography. The crystal structures were determined on an Oxford Diffraction Gemini S Ultra X-ray single-crystal diffractometer using graphite-monochromated MoK\a radiation (λ = 0.71073 Å). The structures were solved by using direct methods or intrinsic methods with the SHELXS-97 and SHELXT-18 program.[1] The Cu metal atoms and many of the nonhydrogen atoms were located according to the direct methods. The positions of the other non-hydrogen atoms were located after refinement by full matrix least-squares by using the SHELXL-14/18program.[2] In the final stage of the least-squares refinement, all non-hydrogen atoms were refined anisotropically. H atoms were generated by SHELXL-14/18 program. The positions of H atoms were calculated based on riding model with thermal parameters that were 1.2 times that of the associated C atoms and participated in the calculation of the final R indices. The structural analysis was performed using Olex2.[3] Crystallographic data (including structure factors) of the structures reported in this paper have been deposited to the Cambridge Crystallographic Data Centre (CCDC) with the depository numbers CCDC **2194952-2194956.**

Computational Details.

The DFT calculations were carried out with the default settings as implemented in ORCA software package (version 5.0.3)[4,5], which incorporates the RIJCOSX[6] for hybrid DFT methods. The geometry optimizations of Cu complexes were performed at B3LYP-D3(BJ)/def2-SVP/def2-TZVP(for Cu) level in gas phase by close-shell (for singlet) or unrestricted open-shell (for other multiplicity) calculations with geometric counterpoise correction (gCP)[7] employed. All optimized geometries were verified by vibrational frequency computations as minima (no imaginary frequency). Figures of HOMO and LOMO were depicted by IboView [8].

Complex **1**, **2**, **3**, and **5** were optimized both at singlet and triplet states. Gibbs free energies indicate that all these complexes have low energy at singlet state. So, further discussions are based on singlet states. Complex **7** was optimized at doublet and quartet states, where doublet state has lower energy level. So complex **7** was discussed as doublet states. SOMO of complex **7** was obtained by biorthogonalization

between alpha and beta orbitals using Multiwfn (3.8 dev).[9]

References:

1. a) G. M. Sheldrick, SHELX97, Programs for Crystal Structure Analysis, Release 97-2, University of Göttingen, Göttingen, Germany, 1997. b) G. Sheldrick, SHELXT - Integrated space-group and crystal-structure determination, *Acta Crystallographica Section A*, 2015, **71**, 3-8.
2. G. Sheldrick, Crystal structure refinement with SHELXL, *Acta Crystallographica Section C*, 2015, **71**, 3-8.
3. O. V. Dolomanov, L. J. Bourhis, R. J. Gildea, J. A. K. Howard and H. Puschmann, OLEX2: a complete structure solution, refinement and analysis program, *J. Appl. Crystallogr.*, 2009, **42**, 339-341.
4. Neese, F. "The ORCA program system" *Wiley Interdisciplinary Reviews: Computational Molecular Science*, 2012, **2**, 73-78.
5. Neese, F. "Software update: the ORCA program system, version 4.0" *Wiley Interdisciplinary Reviews: Computational Molecular Science*, 2017, **8**, e1327.
6. Neese, F.; Wennmohs, F.; Hansen, A.; Becker, U. Efficient, Approximate and Parallel Hartree-Fock and Hybrid DFT Calculations. A 'Chain-Of-Spheres' Algorithm for the Hartree-Fock Exchange. *Chem. Phys*. 2009, **356**, 98-109.
7. H. Kruse, S. Grimme, *J. Chem. Phys.* 2012, **136**, 154101.
8. G. Knizia and J. E. M. N. Klein, Electron Flow in Reaction Mechanisms—Revealed from First Principles, *Angew. Chem. Int. Ed.*, 2015, **54**, 5518-5522.
9. Tian Lu, Feiwu Chen, Multiwfn: A Multifunctional Wavefunction Analyzer, *J. Comput. Chem.* 2012, **33**, 580-592.

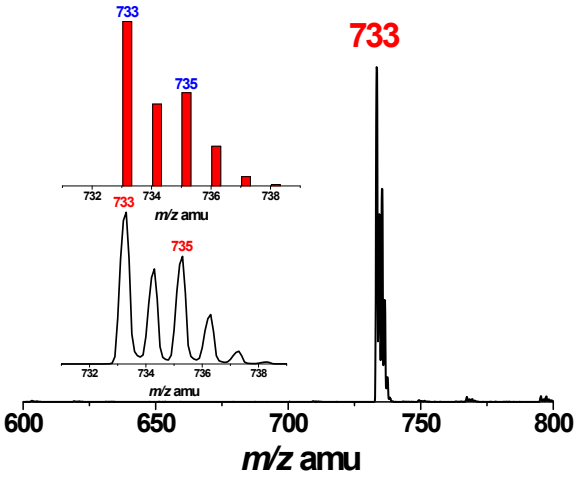

Figure S1. ESI-MS (+ve mode) of **1** in CH_2Cl_2.

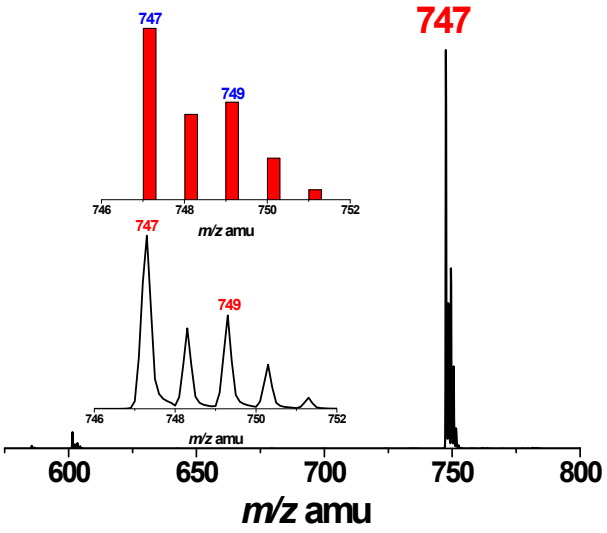

Figure S2. ESI-MS (+ve mode) of **2** in CH_2Cl_2.

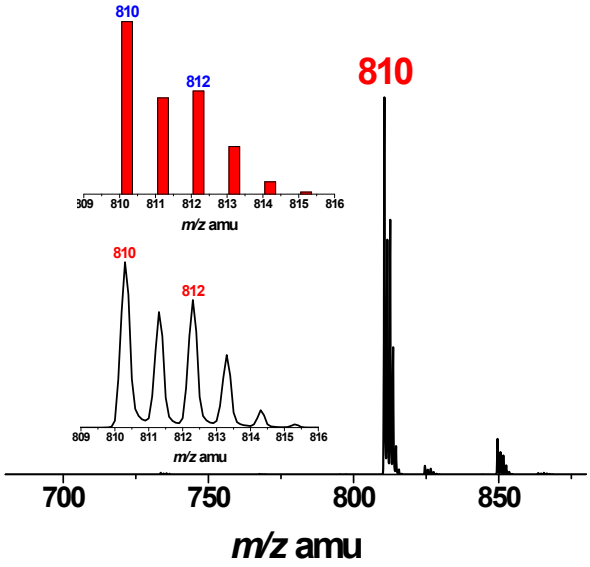

Figure S3. ESI-MS (+ve mode) of **3** in CH_2Cl_2.

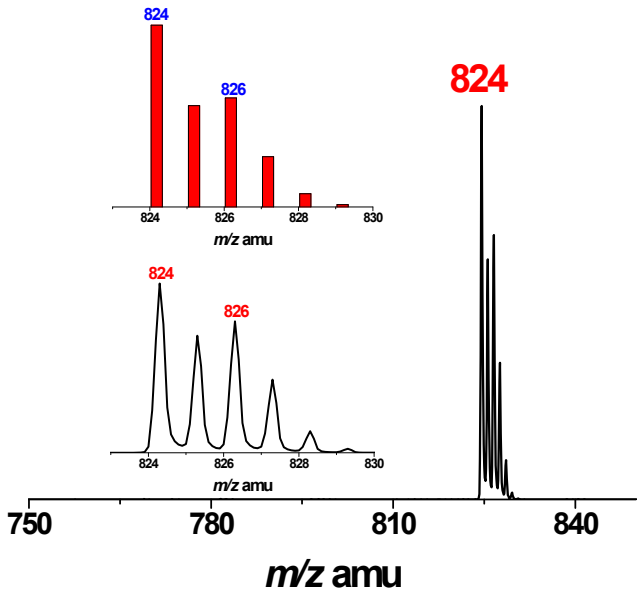

Figure S4. ESI-MS (+ve mode) of **4** in CH_2Cl_2.

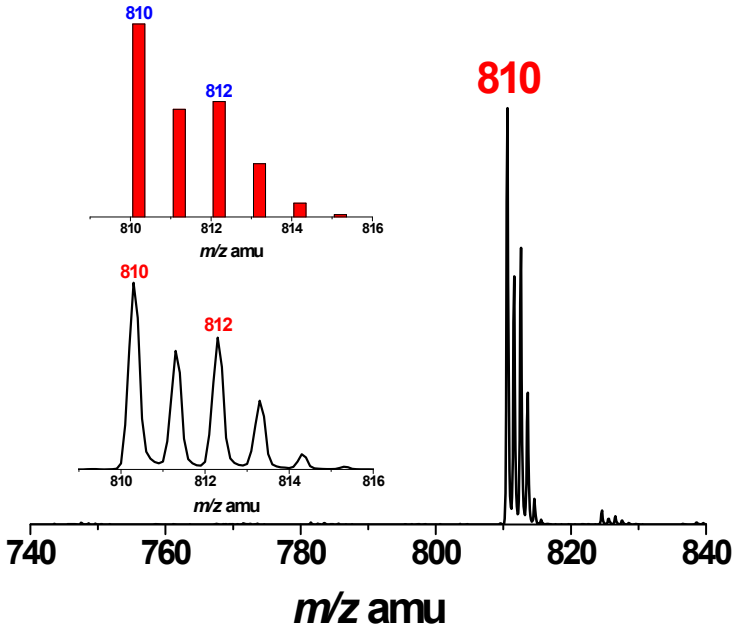

Figure S5. ESI-MS (+ve mode) of **5** in CH_2Cl_2.

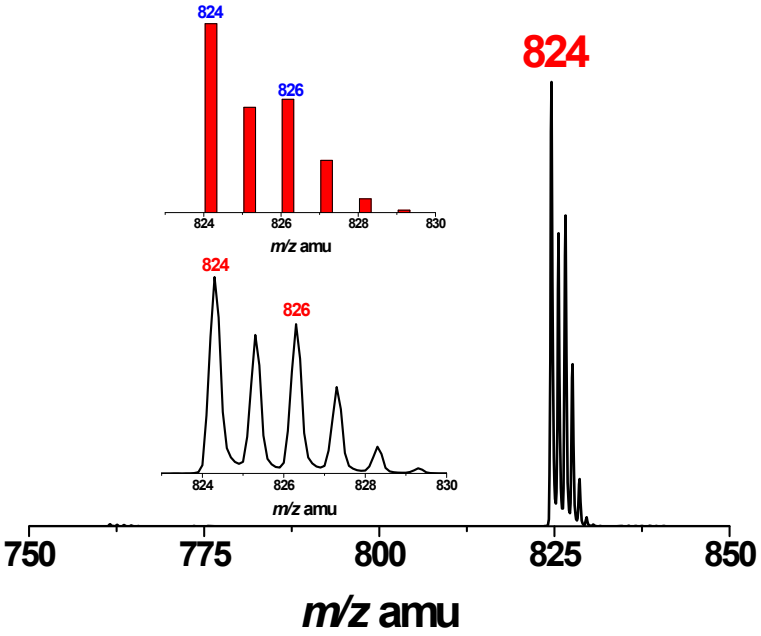

Figure S6. ESI-MS (+ve mode) of **6** in CH_2Cl_2.

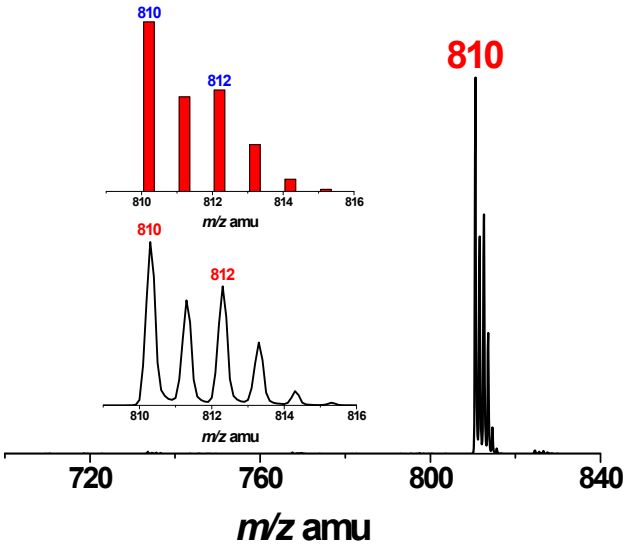

Figure S7. ESI-MS (+ve mode) of **7** in CH_2Cl_2.

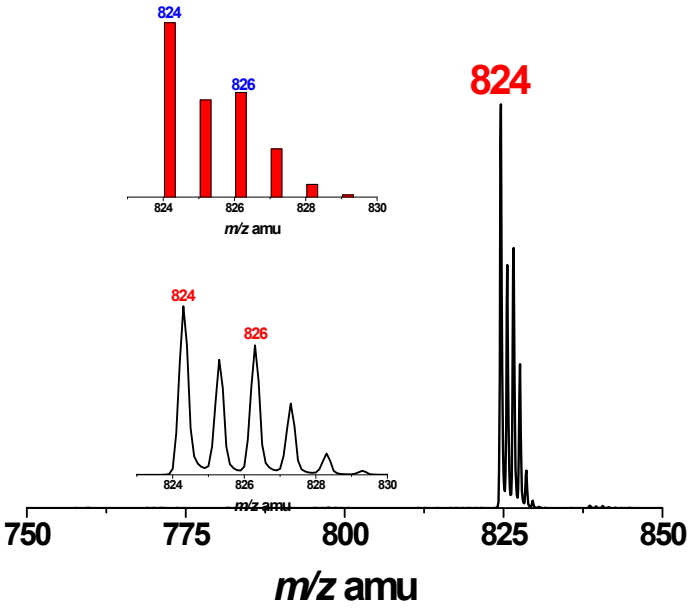

Figure S8. ESI-MS (+ve mode) of **8** in CH_2Cl_2.

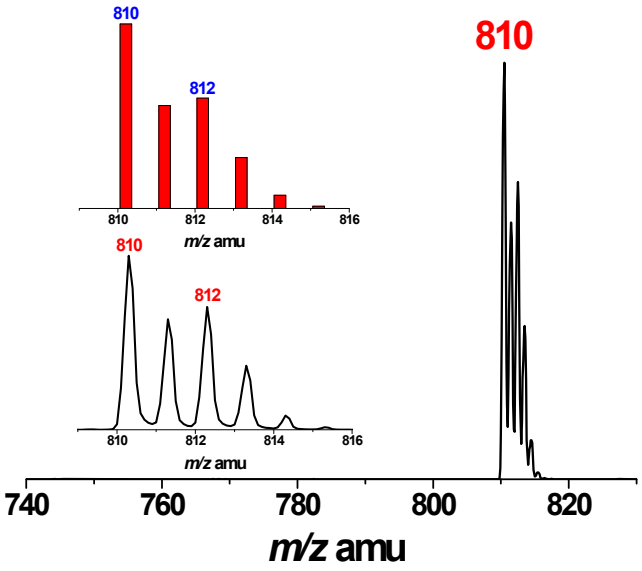

Figure S9. ESI-MS (+ve mode) of **9** in CH_2Cl_2.

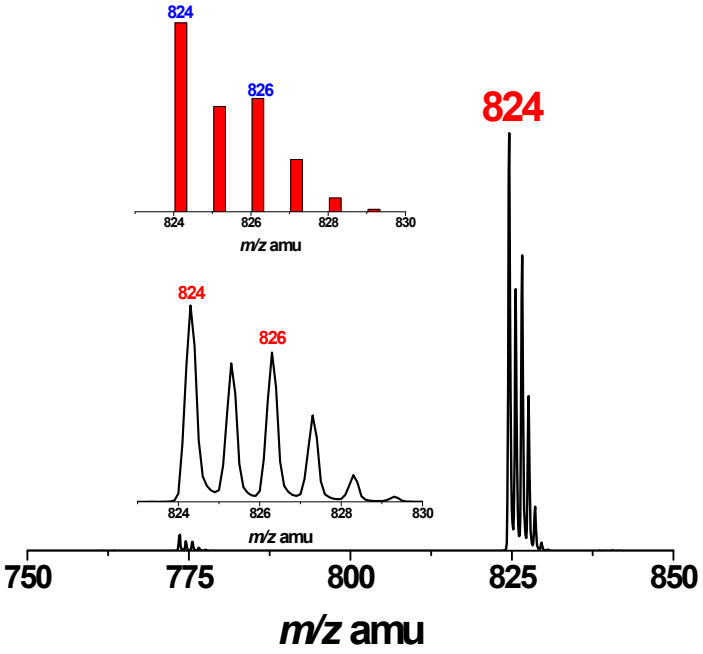

Figure S10. ESI-MS (+ve mode) of **10** in CH_2Cl_2.

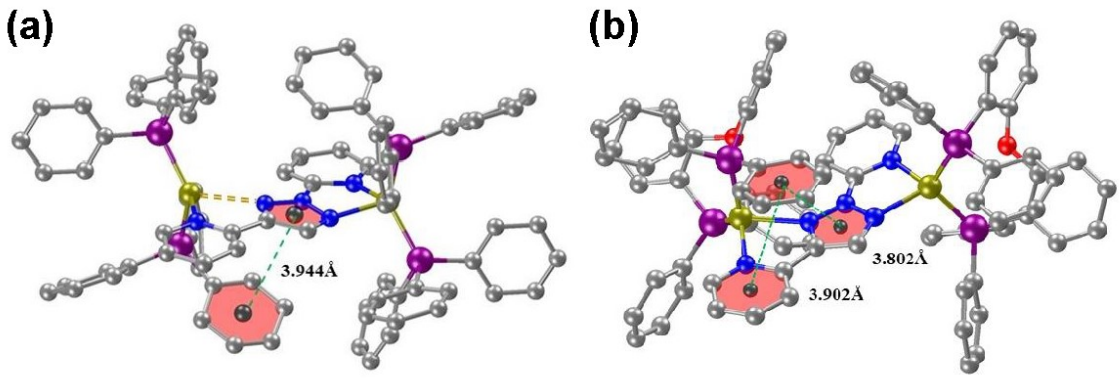

Figure S11. The intra-molecular π-π stacking found in **7** (a) and **8** (b).

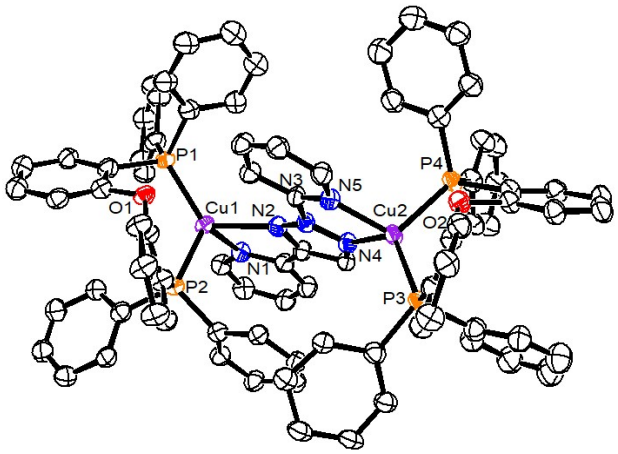

Figure S12. The cationic structure of **8**.

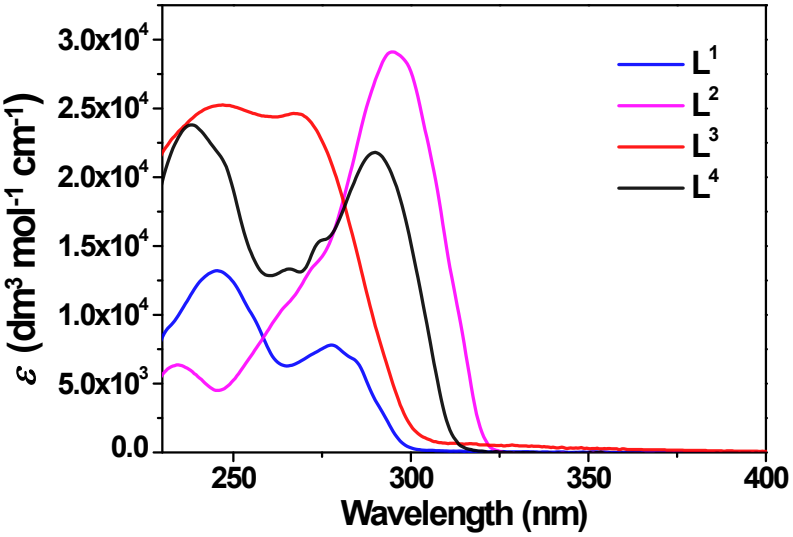

Figure S13. The UV-vis spectra of $\mathbf{L^1}$-$\mathbf{L^4}$ in CH_2Cl_2 at 298 K.

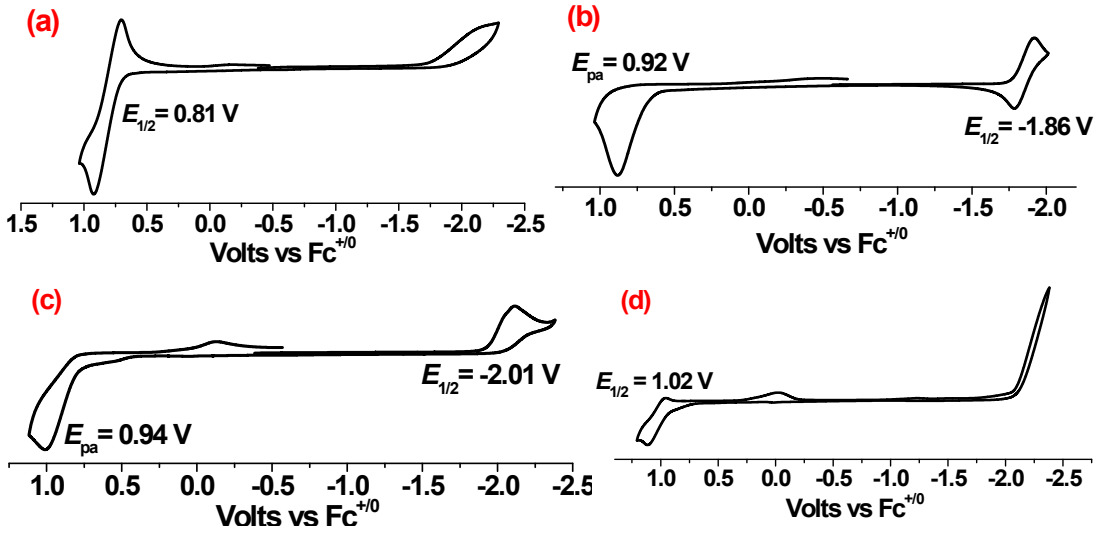

Figure S14. CVs of **2**(a), **4**(b), **9**(c) and **10**(d) in 0.1 *M* $[^nBu_4N]PF_6$ MeCN solutions with a scan rate 0.1

V/s.

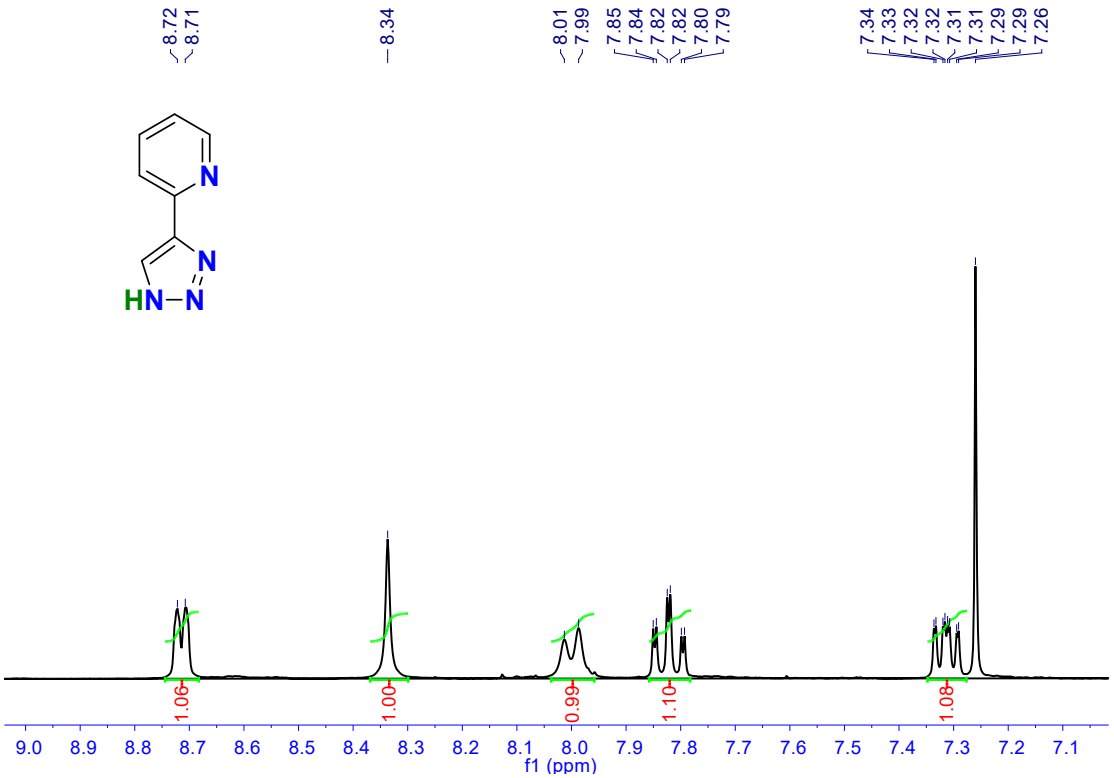

Figure S15. ^{1}H NMR spectrum of **L^{1}** in $CDCl_3$.

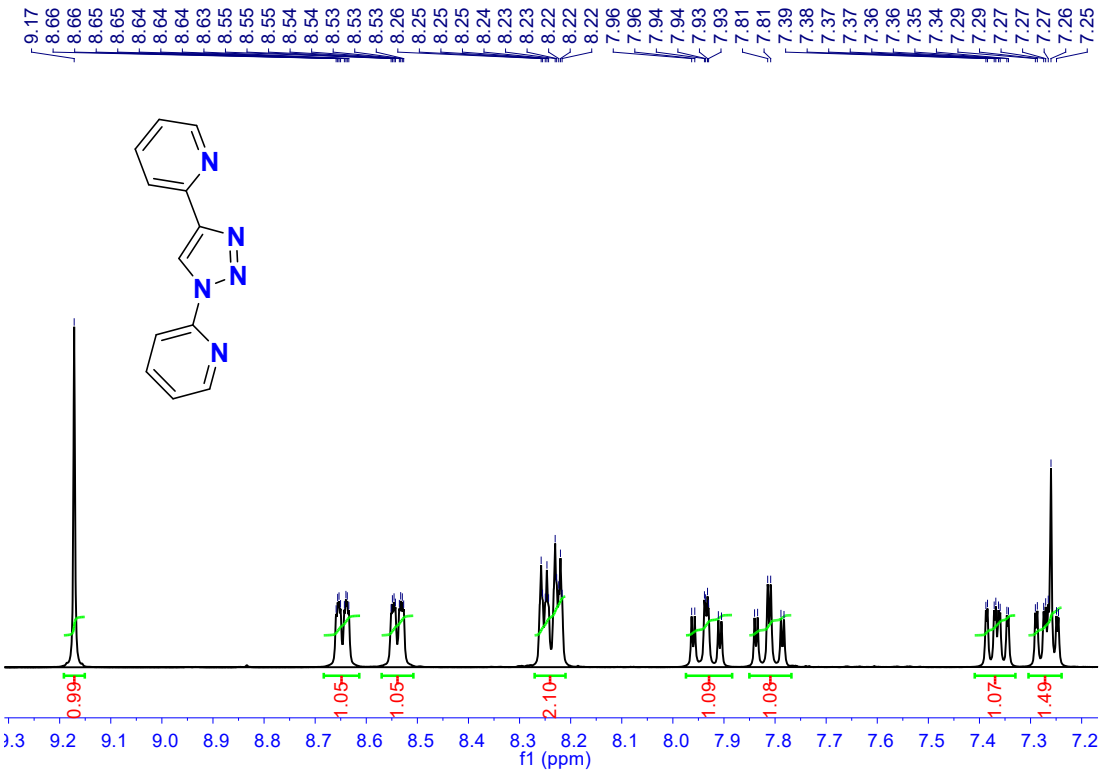

Figure S16. ^{1}H NMR spectrum of **L^{2}** in $CDCl_3$.

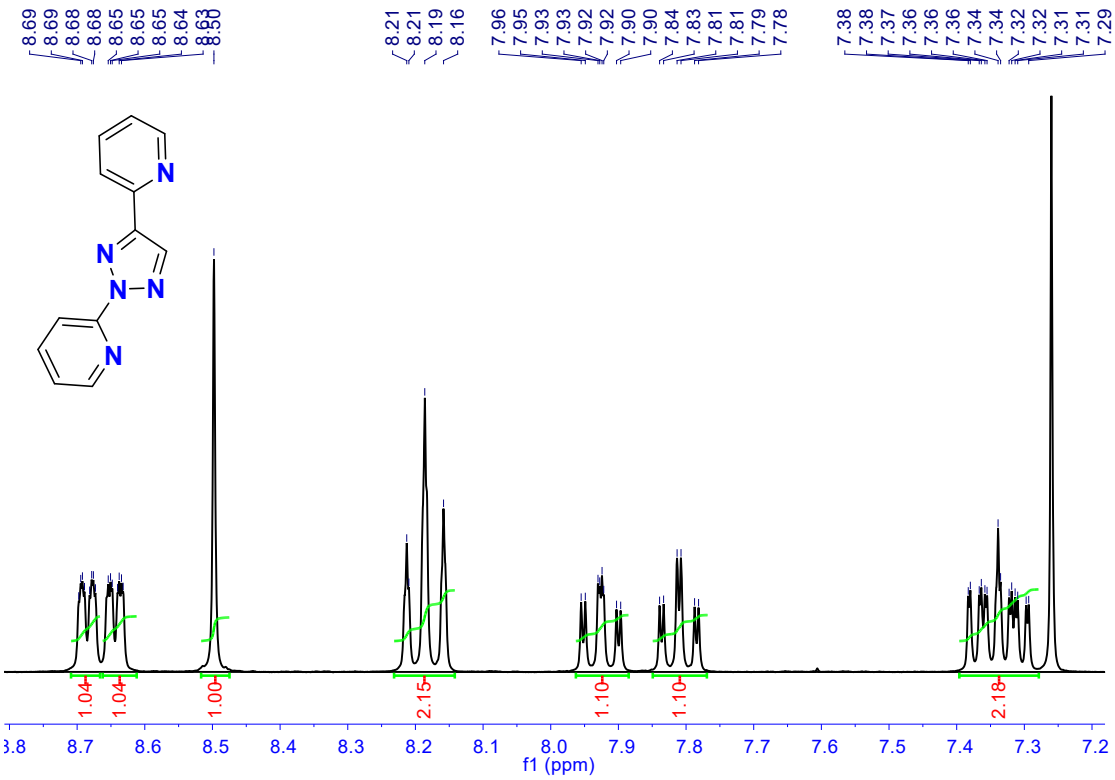

Figure S17. ^{1}H NMR spectrum of **L^{3}** in $CDCl_3$.

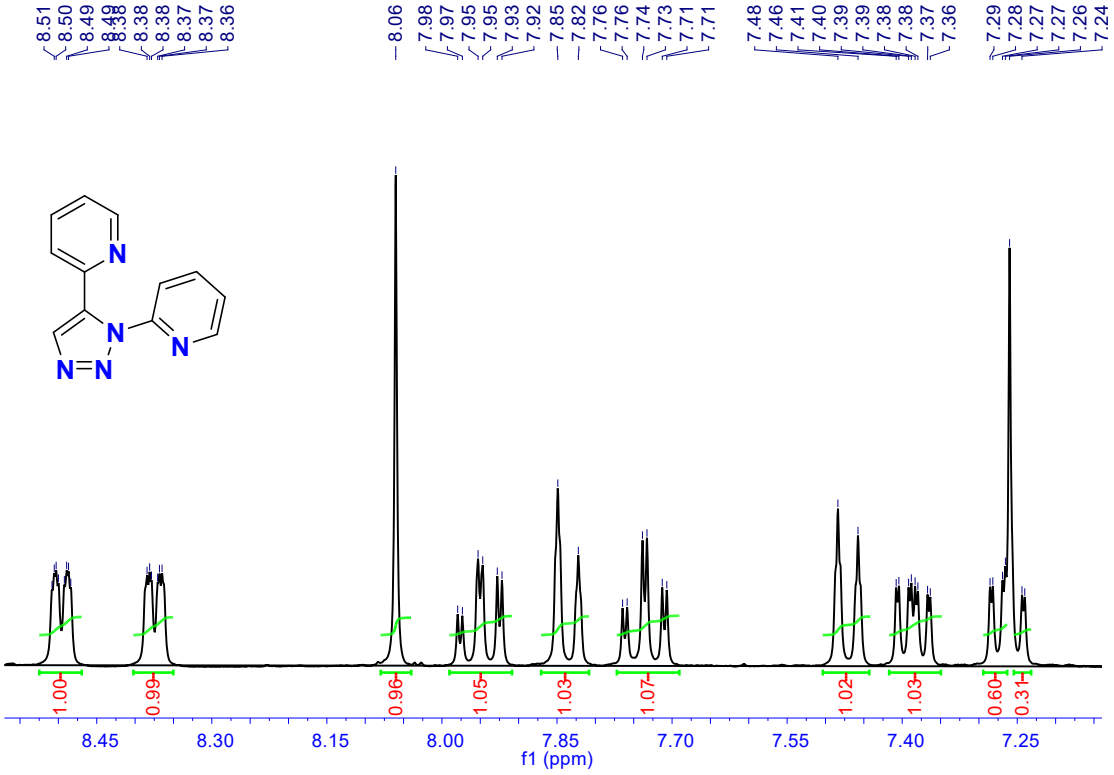

Figure S18. ^{1}H NMR spectrum of **L^{4}** in $CDCl_3$.

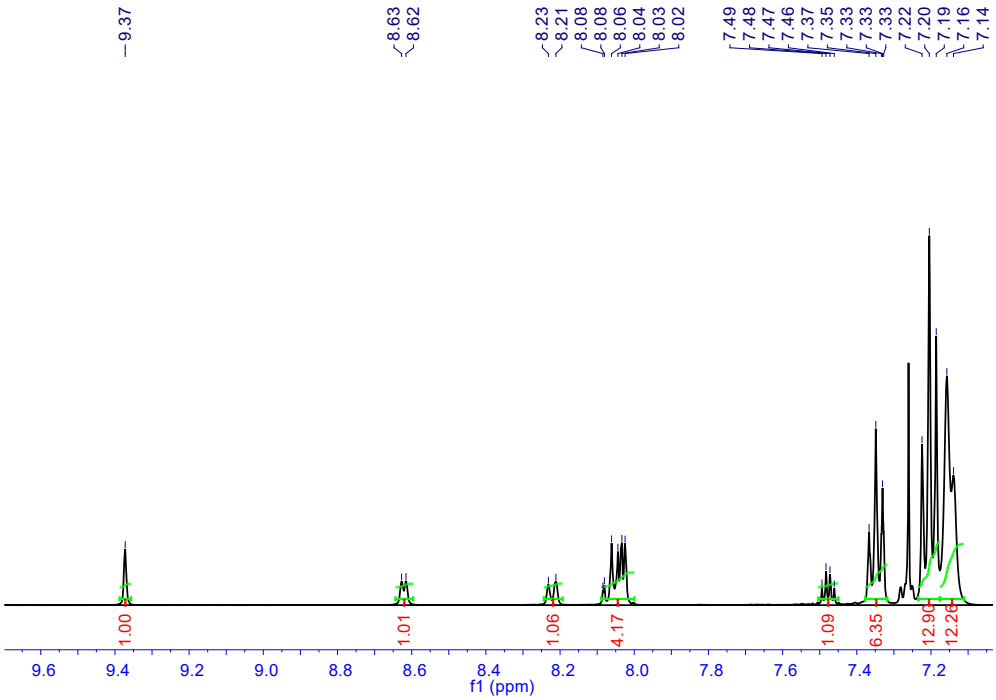

Figure S19. ^{1}H NMR spectrum of **3** in $CDCl_3$.

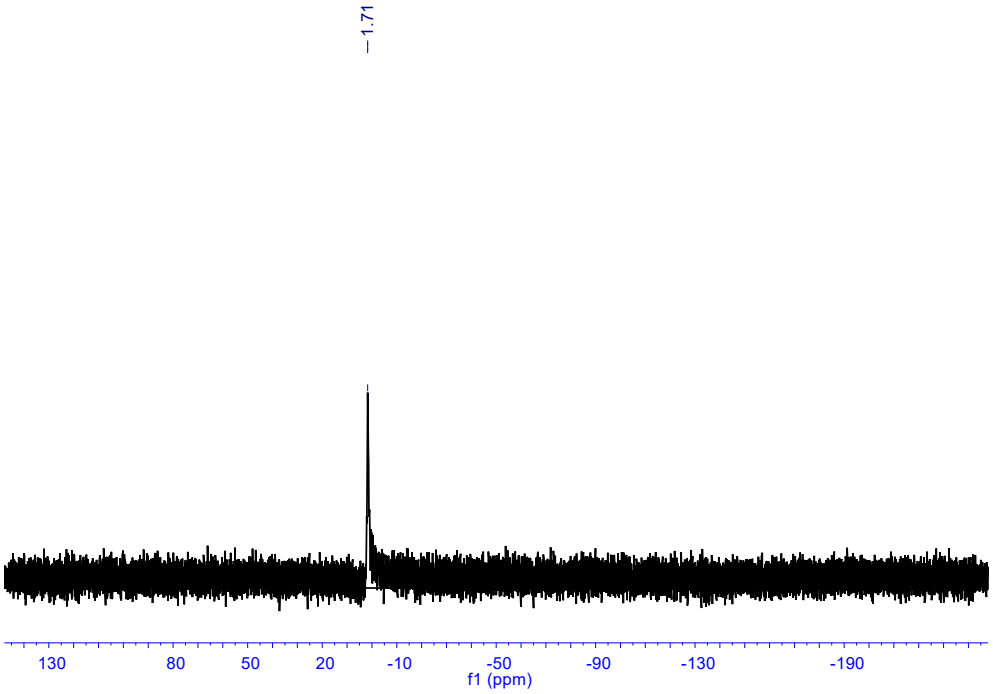

Figure S20. $^{31}P\{^{1}H\}$ NMR spectrum of **3.**

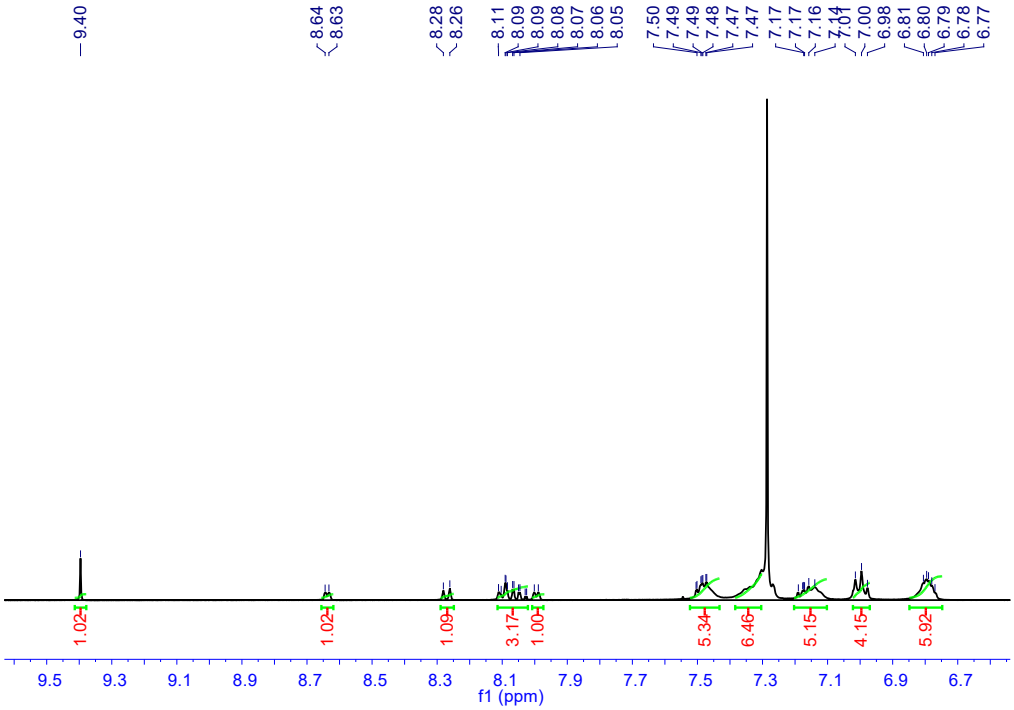

Figure S21. ^{1}H NMR spectrum of **4** in $CDCl_3$.

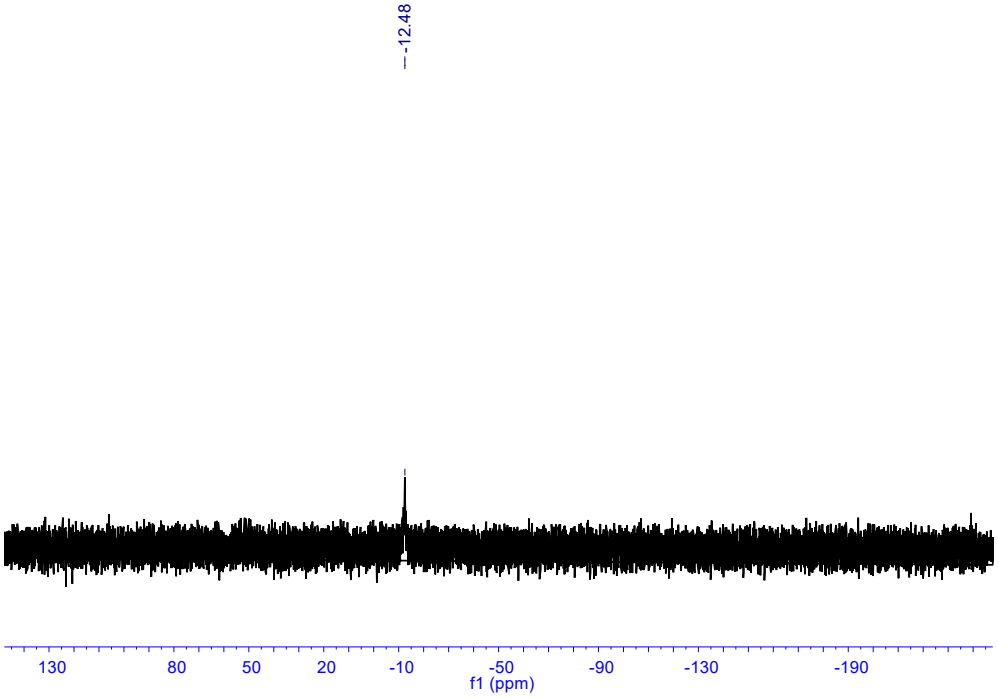

Figure S22. $^{31}P\{^{1}H\}$ NMR spectrum of **4.**

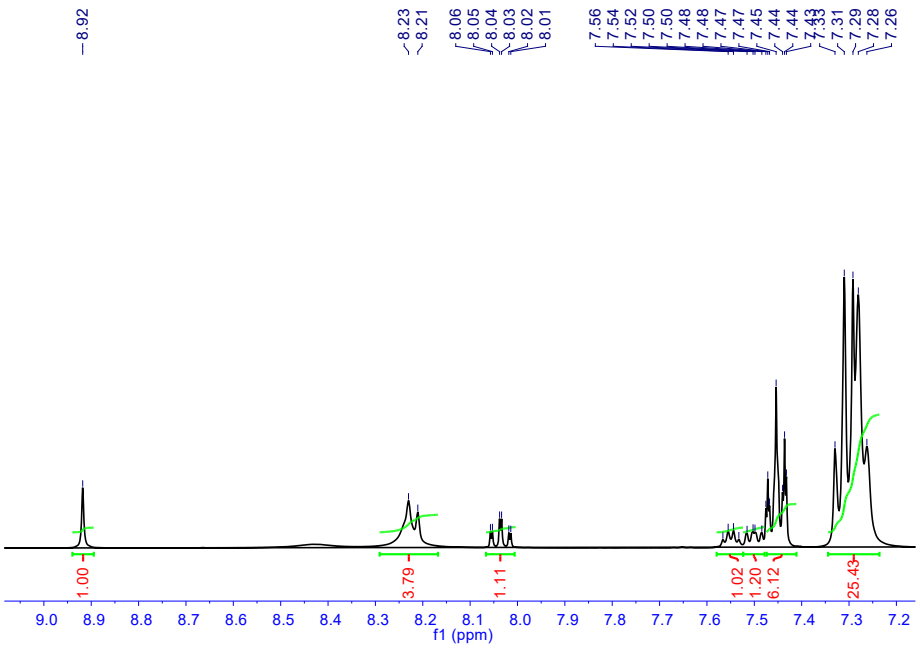

Figure S23. ^{1}H NMR spectrum of **5** in $CDCl_3$.

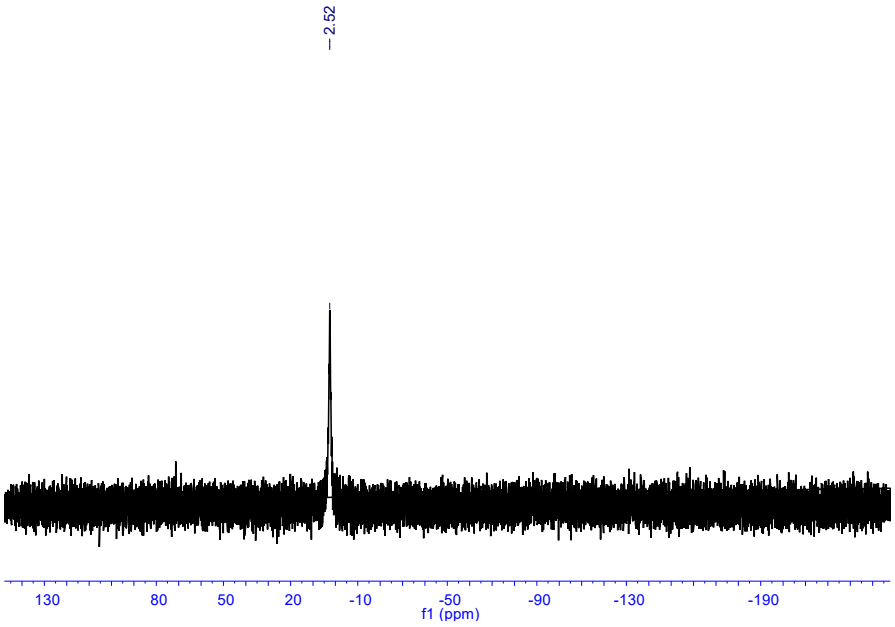

Figure S24. $^{31}P\{^{1}H\}$ NMR spectrum of **5.**

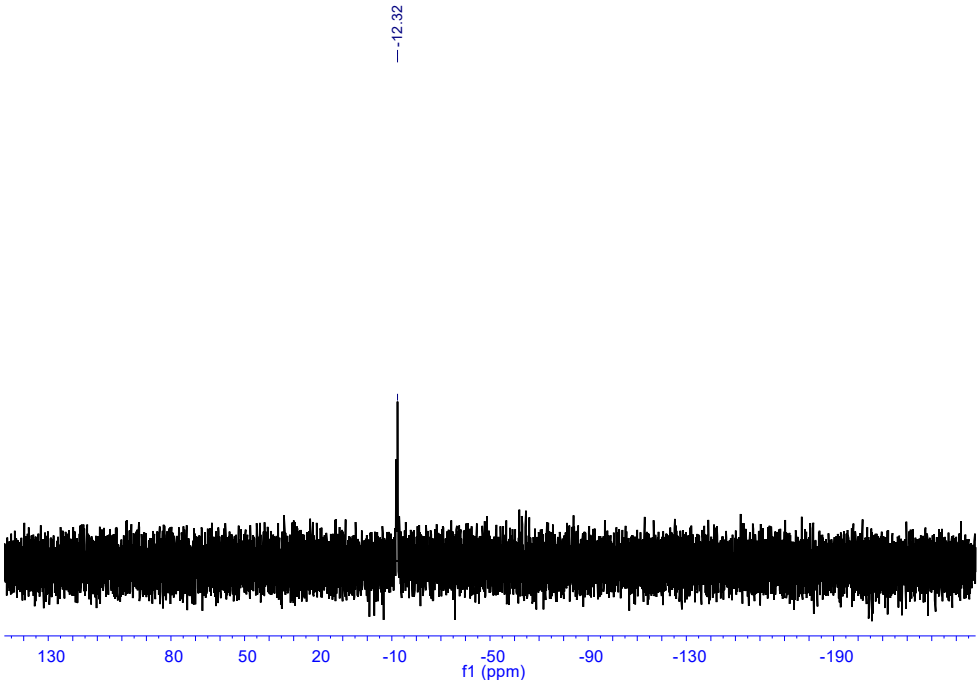

Figure S25. $^{31}P\{^{1}H\}$ NMR spectrum of **6.**

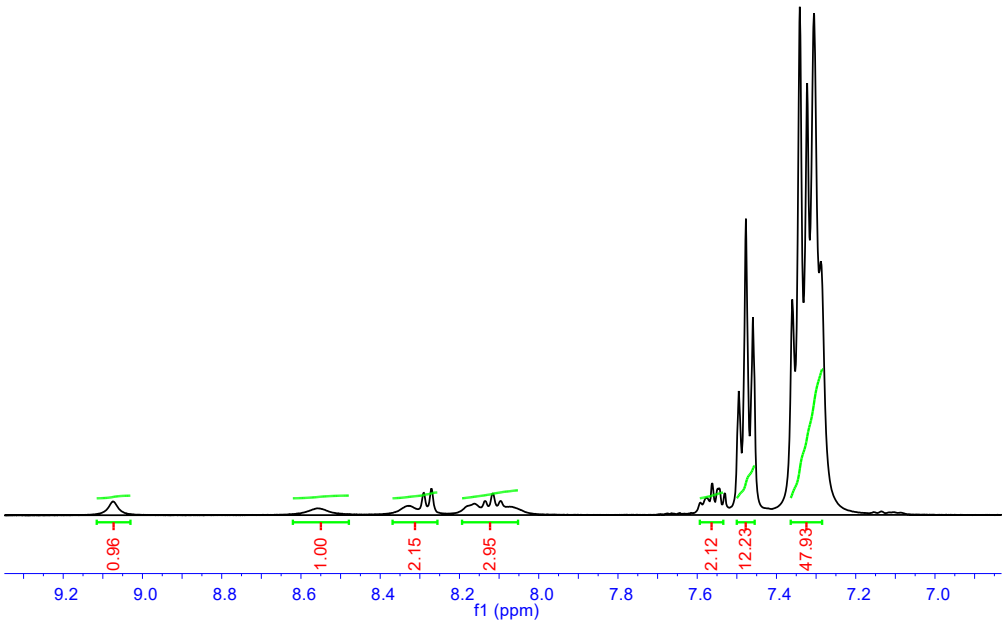

Figure S26. ^{1}H NMR spectrum of **7** in d^{6}-acetone.

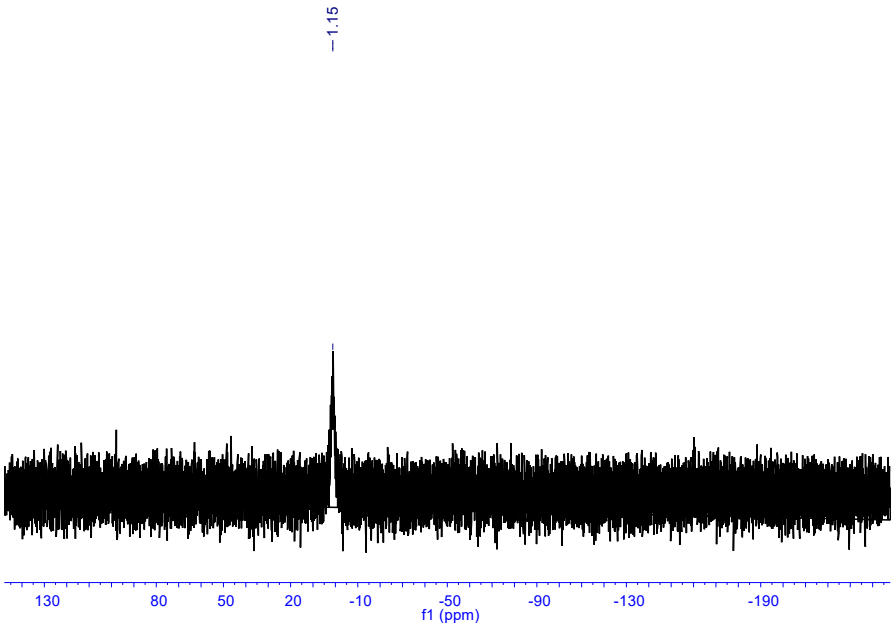

Figure S27. $^{31}P\{^{1}H\}$ NMR spectrum of **7.**

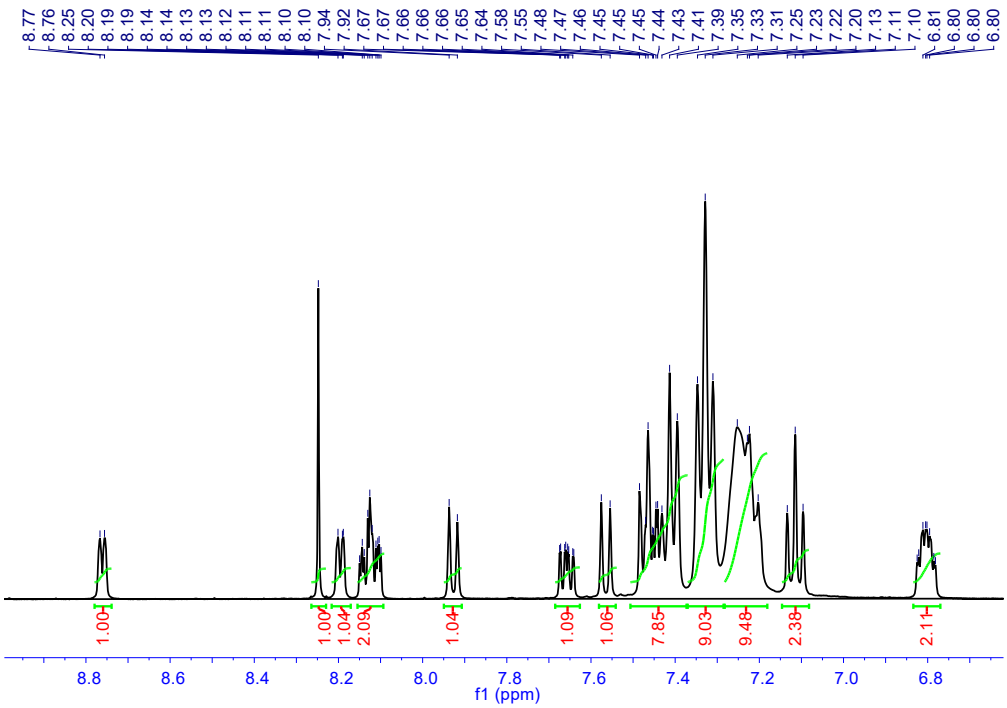

Figure S28. ^{1}H NMR spectrum of **10** in d^{6}-acetone.

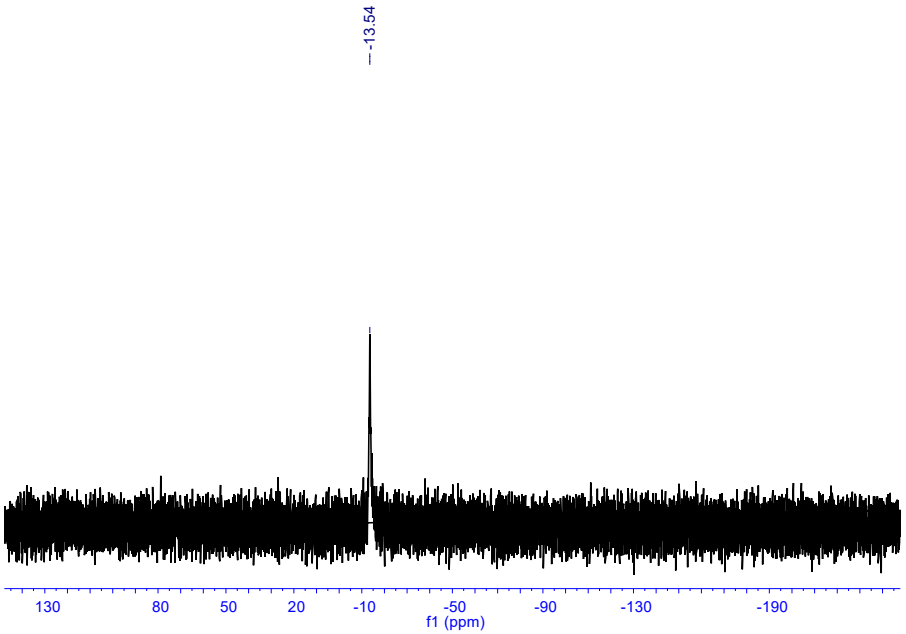

Figure S29. $^{31}P\{^{1}H\}$ NMR spectrum of **10.**

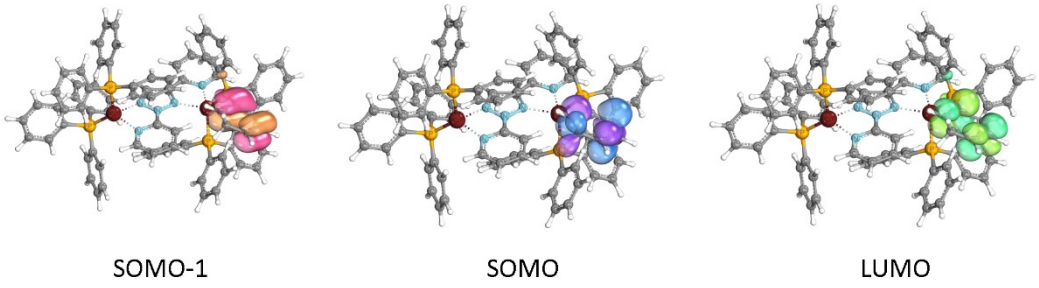

Figure S30. Frontier molecular orbitals for the quartet state of complex **7** calculated at the B3LYP-D3(BJ)/def2-SVP/def2-TZVP(for Cu) level of theory.

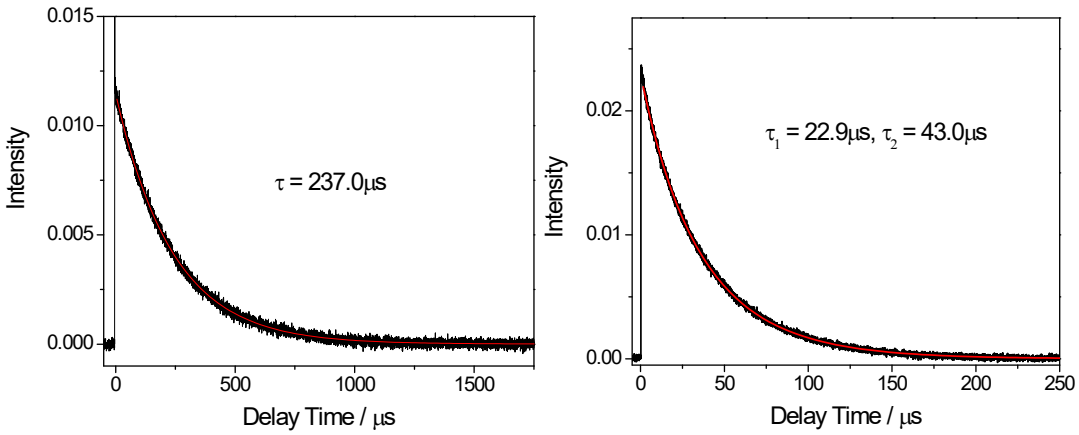

Figure S31. Kinetic time-trace of 77K glassy (left) and 298 K solid (right) state emission of **1**.

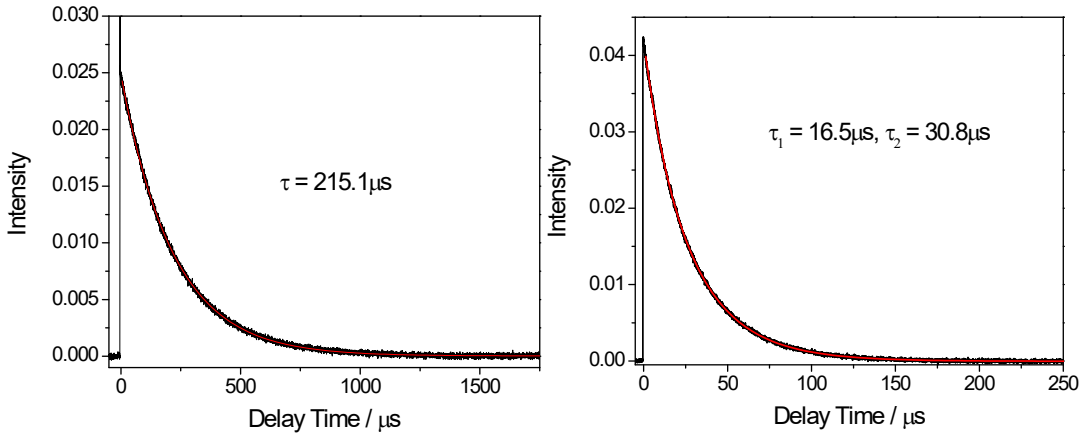

Figure S32. Kinetic time-trace of 77K glassy (left) and 298 K solid (right) state emission of **2**.

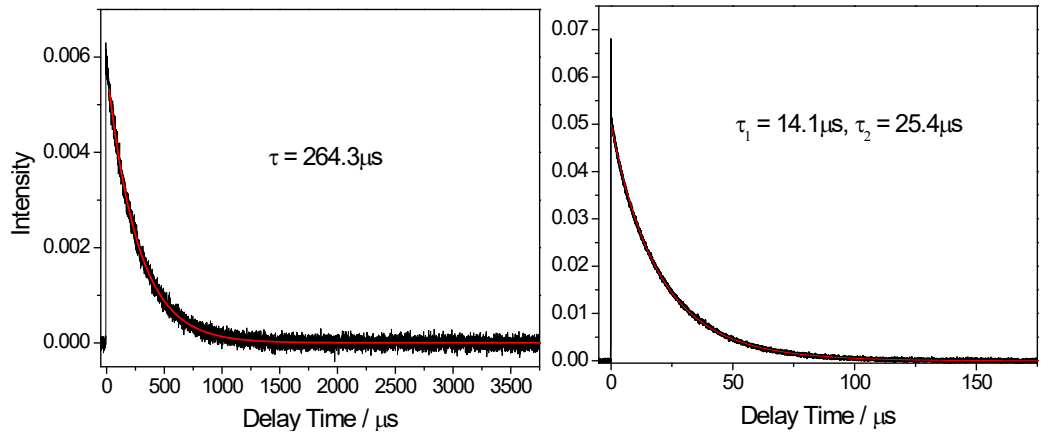

Figure S33. Kinetic time-trace of 77K glassy (left) and 298 K solid (right) state emission of **3**.

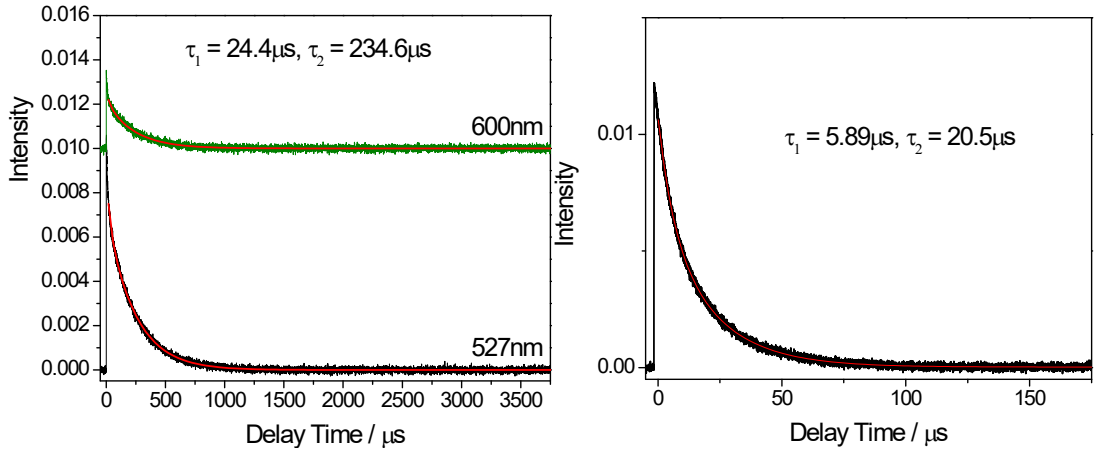

Figure S34. Kinetic time-trace of 77K glassy (left) and 298 K solid (right) state emission of **4**.

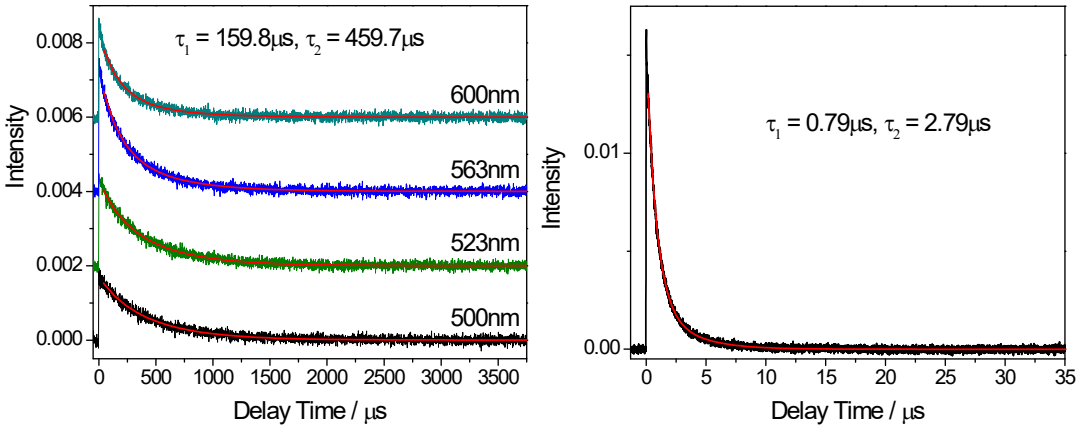

Figure S35. Kinetic time-trace of 77K glassy (left) and 298 K solid (right) state emission of **5**.

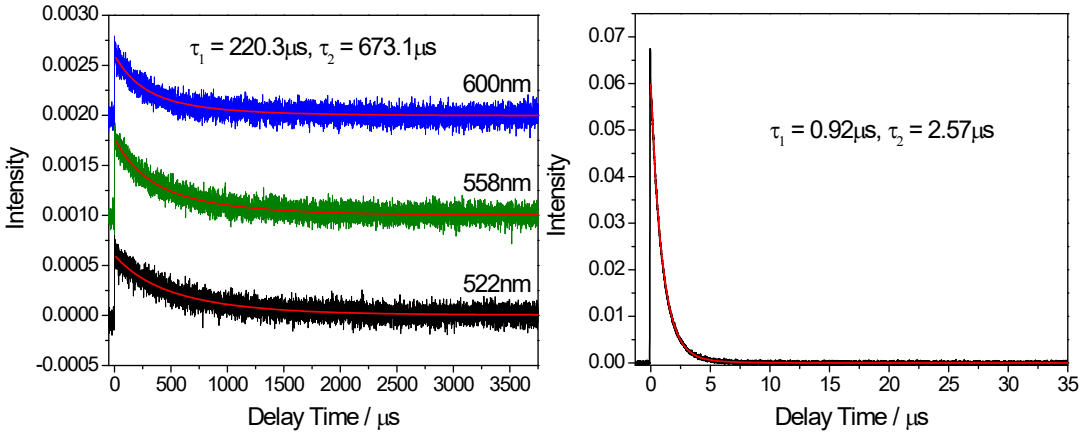

Figure S36. Kinetic time-trace of 77K glassy (left) and 298 K solid (right) state emission of **6**.

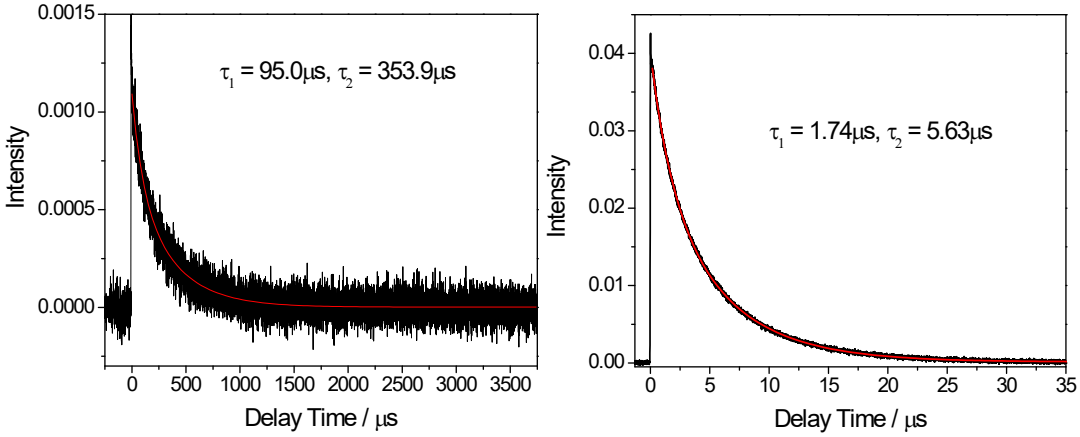

Figure S37. Kinetic time-trace of 77K glassy (left) and 298 K solid (right) state emission of **7**.

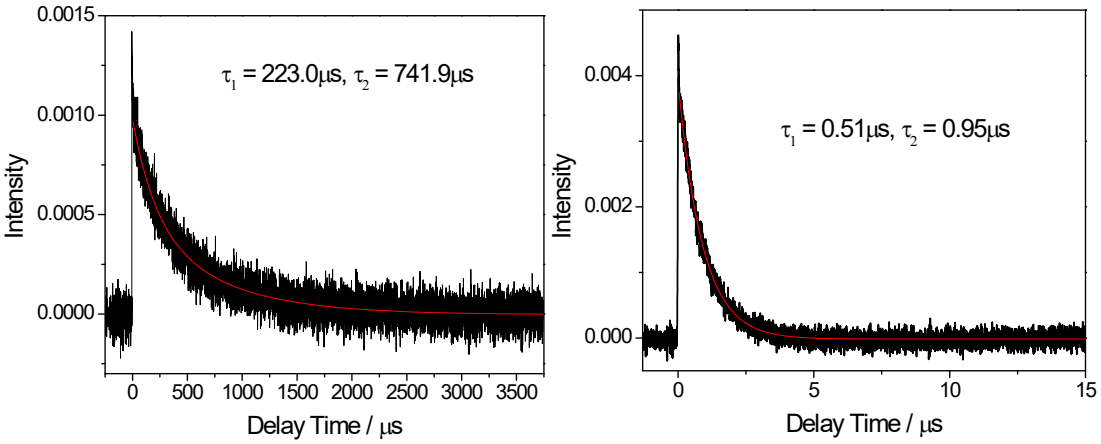

Figure S38. Kinetic time-trace of 77K glassy (left) and 298 K solid (right) state emission of **8**.

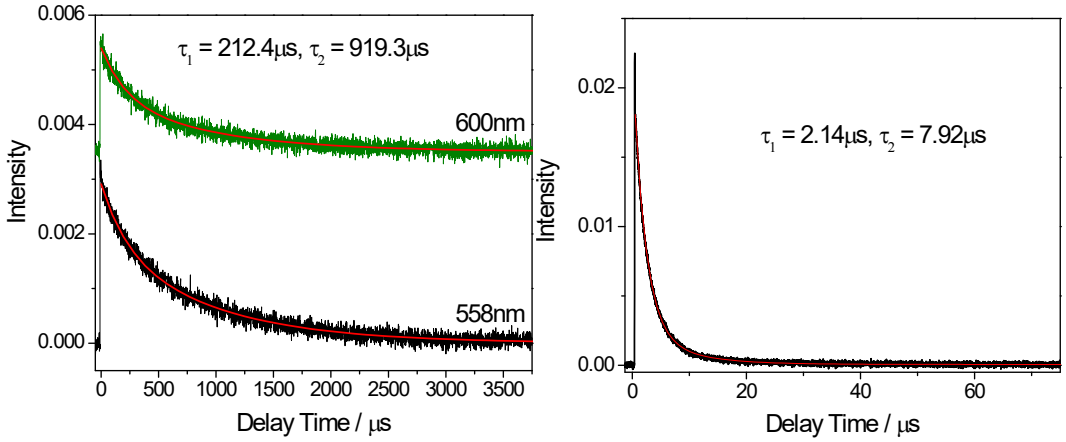

Figure S39. Kinetic time-trace of 77K glassy (left) and 298 K solid (right) state emission of **9**.

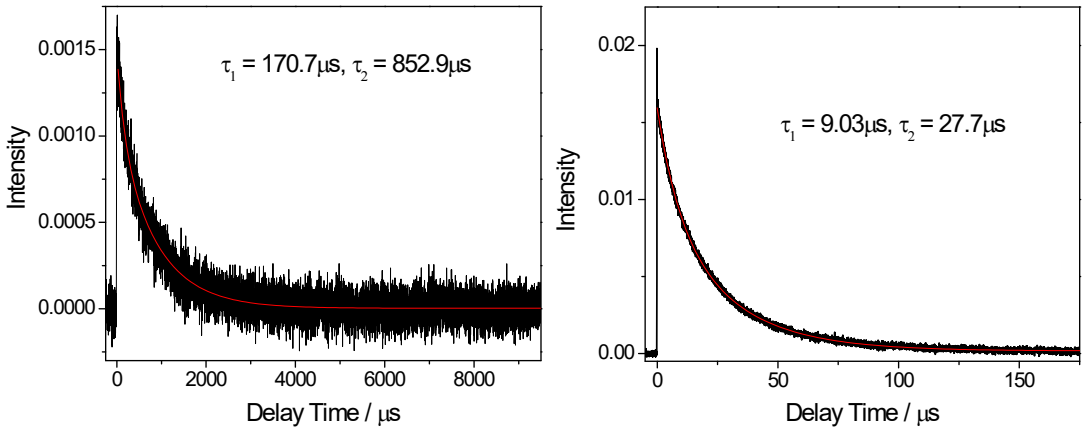

Figure S40. Kinetic time-trace of 77K glassy (left) and 298 K solid (right) state emission of **10**.

Table S1. CV data of Cu(I) compounds **1**-**10**.

complexes	Oxidation $E_{1/2}$ or E_{pa} (vs.$Fc^{+/0}$) [V]	Reduction $E_{1/2}$ or E_{pc} (vs.$Fc^{+/0}$) [V]
1	0.99	-1.86

2	0.8	-1.98
3	0.95	-1.81
4	0.91	-1.86
5	1.04	-1.86
6	0.90	-1.67
7	0.96	-1.66
8	0.90	-1.68
9	0.94	-2.01
10	1.02	-2.08

Table S2. The structural refinement detail for Cu(I) complexes.

	1	**2**	**3**	**5**	**7**
Formula	$C_{43}H_{36}ClCuN_4O_4P_2$	$C_{43}H_{33}ClCuN_4O_5P_2$	$C_{48}H_{39}ClCuN_5O_4P_2$	$C_{48}H_{39}ClCuN_5O_4P_2$	$C_{84}H_{70}Cl_2Cu_2N_5O_8P_4$
Mr	833.69	847.67	910.77	910.77	1599.31
T /K	293 (2)	293 (2)	293 (2)	100.0 (1)	153 (2)
Crystal syst.	Triclinic	Monoclinic	Triclinic	Triclinic	Triclinic
Space group	*P*-1	$P2_1/n$	*P*-1	*P*-1	*P*1
a/Å	11.6082 (9)	11.535 (3)	11.5602 (10)	11.1772 (5)	12.809 (3)
b/Å	12.6678 (14)	25.303 (6)	12.5310 (11)	12.5873 (6)	13.334 (3)
c/Å	14.4672 (11)	14.450 (3)	16.7292 (15)	15.9561 (9)	13.599 (3)
α, (°)	96.310 (8)	90	73.984 (8)	83.654 (4)	111.45 (3)
β, (°)	109.918 (7)	98.253 (5)	76.055 (7)	71.934 (5)	91.19 (3)
γ, (°)	94.522 (8)	90	68.717 (8)	86.100 (4)	113.60 (3)
V/ Å^3	1972.6 (3)	4173.8 (17)	2143.5 (4)	2119.77 (19)	1942.5 (9)
Z	2	4	2	2	1
ρ_{calcd} / Mg m^{-3}	1.404	1.349	1.411	1.427	1.367
F(000)	860	1744	940	940	825
Collected refl.	14066	65399	23586	13987	56296
Unique refl.	6944	9694	7536	7468	17416
R(int)	0.073	0.040	0.047	0.032	0.059
Final *R* indices, $I > 2\sigma(I)$	R_1(obs) = 0.076 *w*R(all) = 0.193	R_1(obs) =0.064 *w*R(all) = 0.2044	R_1(obs) = 0.05 *w*R(all) =0.132	R_1(obs) = 0.042 *w*R(all) = 0.096	R_1(obs) = 0.085 *w*R(all) = 0.280
GOF	1.05	1.04	1.08	1.04	1.04
No.of par.	500	587	587	550	779

Table S3. Frontier orbital energies for the ground state of **1**, **2**, **3**, **5**, and **7** in eV.

complex	**1**	**2**	**3**	**5**	**7**
LUMO	-4.265043 eV	-4.267560 eV	-4.213231 eV	-4.553398 eV	-6.725309 eV
HOMO	-7.907280 eV	-7.902824 eV	-7.838501 eV	-7.996391 eV	-8.591231 eV
Energy gap	3.642237 eV	3.635265 eV	3.62527 eV	3.442993 eV	1.865922 eV